Recycling and Reuse Technology Transfer Center

http://www.rrttc.uni.edu

Gas Phase Reactions of Conjugated Dienes as a Model for Pyrolysis Product Information

Publication: 1993 – 005

Michaela Rich, Michelle Hammer, Tim Burrell, Curtiss Hanson

93-005

GAS PHASE REACTIONS OF CONJUGATED DIENES AS A MODEL FOR PYROLYSIS PRODUCT FORMATION Michaela L. Rich, Michelle D. Hammer, Tim Burrell, Curtiss D. Hanson; Department of Chemistry, University of Northern Iowa, Cedar Falls, IA, 50614-0423

The pyrolysis of styrene-butadiene rubber (SBR) produces large molecular weight aromatic hydrocarbons through secondary reactions in the gas phase. Fourier transform ion cyclotron resonance mass spectrometry (FT-ICR) was used to analyze the products produced by the gas phase reactions that occur during the pyrolysis of SBR tires. Conjugated diene systems were used on the FT-ICR as models for these reactions in order to better understand the process through which secondary pyrolysis products are formed. Relative rates of reaction and product distribution of the conjugated diene systems will be shown to be consistent with those from the SBR tire pyrolysis.

93-005

GAS PHASE REACTIONS OF CONJUGATED DIENES AS A MODEL FOR PYROLYSIS PRODUCT FORMATION Michaela L. Rich, Michelle D. Hammer, Tim Burrell, Curtiss D. Hanson; Department of Chemistry, University of Northern Iowa, Cedar Falls, IA, 50614-0423

The pyrolysis of styrene-butadiene rubber (SBR) produces large molecular weight aromatic hydrocarbons through secondary reactions in the gas phase. Fourier transform ion cyclotron resonance mass spectrometry (FT-ICR) was used to analyze the products produced by the gas phase reactions that occur during the pyrolysis of SBR tires. Conjugated diene systems were used on the FT-ICR as models for these reactions in order to better understand the process through which secondary pyrolysis products are formed. Relative rates of reaction and product distribution of the conjugated diene systems will be shown to be consistent with those from the SBR tire pyrolysis.

GAS PHASE REACTIONS OF CONJUGATED DIENES AS A MODEL FOR PYROLYSIS PRODUCT FORMATION

Michaela L. Rich, Michelle D. Hammer, Tim Burrell, Curtiss D. Hanson

Department of Chemistry, University of Northern Iowa, Cedar Falls, IA 50614-0423

Abstract

The pyrolysis of styrene-butadiene and poly isoprene rubber produces large molecular weight aromatic hydrocarbons through secondary reactions in the gas phase. Fourier transform ion cyclotron resonance mass spectrometry (FT-ICR) was used to analyze the products produced by the gas phase reactions that occur during the pyrolysis of tires. Conjugated diene systems were used on the FT-ICR as models for these reactions in order to better understand the process through which secondary pyrolysis products are formed. Relative rates of reaction and product distribution of the conjugated diene systems will be shown to be consistent with those from the tire pyrolysis.

INTRODUCTION

The large amount of scrap automobile tires contained in landfills has become a major environmental concern in recent years. Pyrolysis, or thermal decomposition in the absence of oxygen, provides an effective means of cleaning up the environment by eliminating the used tires in landfills and recovering the steel they contain for reuse elsewhere (1).

Pyrolysis produces a complicated distribution of aromatic and aliphatic hydrocarbons (1,2,3,4). An understanding of the reaction mechanisms that lead to the formation of these hydrocarbons allows for a better understanding of what forms soot and how it is produced. This is necessary in order to determine if soot formation can be controlled, or if the products can be recycled and put back into the pyrolysis process as fuel for the pyrolysis oven. Work has been done by Pakdel (4) utilizing Fourier transform infrared spectroscopy (FT-IR) and gas chromatography mass spectrometry (GC-MS) in order to analyze the liquid fraction of pyrolysis products. Although this method provides a clear picture of the product distribution, it is too slow when analyzing reactions which occur in the gas phase. No information regarding the mechanism of gas phase product formation can be provided.

Fourier transform ion cyclotron resonance mass spectroscopy (FT-ICR) provides an excellent analytical technique which gives quantitative and qualitative information regarding gas phase ion/molecule reaction pathways. Experiments are conducted in a low pressure atmosphere ca. 2×10^{-7} torr, which maintains a low ion concentration and

collision rate. Reactions can be observed at increments of 0.001 milliseconds. This allows gas phase reactions to be closely monitored to gain understanding of the mechanisms of product formation. The benefits of FT-ICR and its analytical capabilities regarding ion molecule reactions in the gas phase have been discussed elsewhere (5,6,7,8,9).

Much work has been done on the reactions leading to the formation of soot particles during combustion/fuel pyrolysis processes using a standard acetylene oxygen flame (2,3,10,11,12,13,14,15,16,17,18,19) An ionic mechanism has been proposed by Calcote (2,3) as soot is only found in flames of carbon containing fuels that produce ions (3). A flowchart of the mechanism, contained in Figure 1, shows the process by which small unsaturated hydrocarbons form larger polycyclic and substituted hydrocarbons through subsequent ion/molecule reactions. These hydrocarbons provide the basis for the larger soot aggregates produced during combustion.

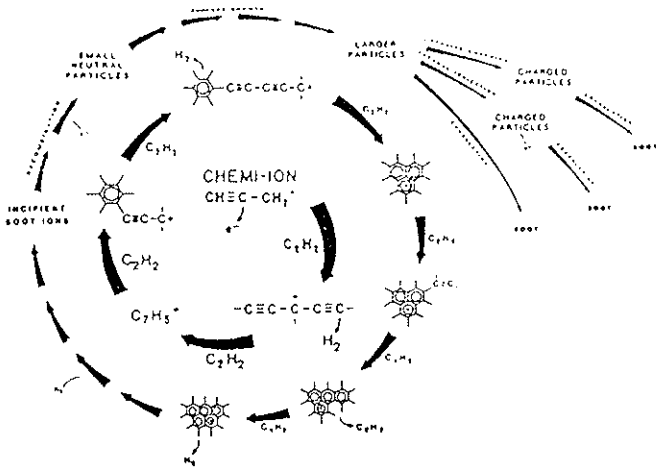

Figure 1. Flowchart for the ionic mechanism of soot formation

In the mechanism, the $C_3H_3^+$ cation is believed to be the major precursor ion due to its high abundance in sooting flames (2,3,10,11,12,13,14,15,16,17). The $C_3H_3^+$ cation is postulated to be formed in fuel rich flames through the following reactions (2,3)

$$CH + O \rightarrow CHO^+ + e- \quad (1)$$

$$CHO^+ + H_2O \rightarrow H_3O^+ + CO \quad (2)$$

$$H_3O^+ + C_3H_2 \rightarrow C_3H_3^+ + H_2O \quad (3)$$

Following formation, the $C_3H_3^+$ cation forms larger hydrocarbons which continue to react with acetylenes and diacetylenes in subsequent ion/molecule reactions.

$$C_3H_3^+ + C_2H_2 \rightarrow C_5H_3^+ + H_2 \quad (4)$$

$$C_5H_3^+ + C_2H_2 \rightarrow C_7H_5^+ \quad (5)$$

$$C_7H_5^+ + C_2H_2 \rightarrow C_9H_7^+ \quad (6)$$

$$C_9H_7^+ + C_2H_2 \rightarrow C_{11}H_9^+ \quad (7)$$

$$C_9H_7^+ + CH_2 \rightarrow C_{13}H_{11}^+ \quad (8)$$

Additional ions observed by Calcote, produced in an acetylene/oxygen flame are found in Table 1 (2). Carbon-hydrogen ratios of the ions involved require that they be aromatic rings (3).

John Eyler and others (15,16,17) have effectively used FT-ICR to model the reactions of the two isomers of the $C_3H_3^+$ cation regarding the cation's role as an aromatic precursor during soot formation. Specifically, reactions of the $C_3H_3^+$ cation with acetylene, diacetylene, and dueteroacetylene have been investigated to gain understanding of the process whereby the reactive propargyl $C_3H_3^+$ isomer is converted to the unreactive cyclopropenylium isomer (16).

$$l\text{-}C_3H_3^+ + C_2H_2 \rightarrow [\, C_5H_5^+ \,] \rightarrow c\text{-}C_3H_3 + C_2H_2 \quad (9)$$

TABLE 1

Ions Observed in Sooting Acetylene-Oxygen Flames

Molecular Weight	Formula	Suggested Structure
39	$C_3H_3^+$	
51	$C_4H_3^+$	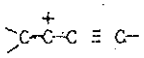
53	$C_4H_5^+$	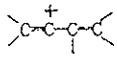
63	$C_5H_3^+$	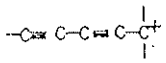
65	$C_5H_5^+$	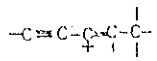
75	$C_6H_3^+$	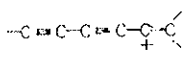
77	$C_6H_5^+$	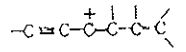
79	$C_6H_7^+$	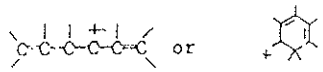
89	$C_7H_5^+$	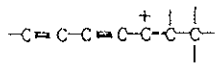
91	$C_7H_7^+$	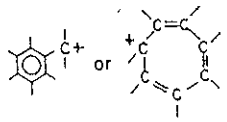
103	$C_8H_7^+$	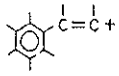
115	$C_9H_7^+$	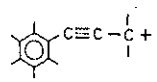

In order to gain additional information about the role of the $C_3H_3^+$ cation in the mechanism of soot formation, reactions of the $C_3H_3^+$ cation with aromatics have been studied.

$$C_3H_3^+ + C_6H_6 \rightarrow C_6H_6^+ + C_3H_3 \quad (10)$$

$$C_3H_3^+ + C_6H_6 \rightarrow C_7H_7^+ + C_2H_2 \quad (11)$$

$$C_3H_3^+ + C_6H_6 \rightarrow C_9H_7^+ + H_2 \quad (12)$$

Reactions with alcohols have also been investigated in order to determine their significance in reducing soot formation (17).

$$C_3H_3^+ + CH_3OH \rightarrow CH_3OH_2^+ + C_3H_2^+ \quad (13)$$

The majority of the previous work regarding the mechanism of soot formation focuses on two isomers of the $C_3H_3^+$ cation and the formation of polycyclic aromatics during combustion processes. Bowser and Weinberg (2,3,20) have postulated that during pyrolysis the $C_3H_3^+$ cation is formed according to reaction 14.

$$C_2 + CH_3 \rightarrow C_3H_3^+ + e^- \quad (14)$$

However, little attention has been given to reactions that occur during the pyrolysis process, particularly the mechanism by which the $C_3H_3^+$ cation produces larger aliphatic hydrocarbons during soot formation.

This research centers around modeling the gas phase reactions that occur during pyrolysis in order to gain a better understanding of the mechanisms by which pyrolysis products are formed. Conjugated diene ionic models were analyzed using FT-ICR to model both aliphatic and aromatic production. Two types of reactions will be discussed: i) reactions in which the $C_3H_3^+$ cation acts as a precursor to aromatic systems; ii)

reactions in which the $C_3H_3^+$ cation produces the molecular ion of the neutral target gas through charge exchange. Further collisions of the molecular ion with the neutral gas result in a product distribution of larger substituted aliphatic systems.

Product rate and distribution of the pyrolysis products will be shown to be consistent with the aliphatic production that takes place in the reactions of larger substituted conjugated diene systems.

EXPERIMENTAL

All experiments were performed on an IonSpec OMEGA 50 Fourier transform ion cyclotron resonance mass spectrometer (FT-ICR) with a high field Walker Scientific electromagnet held at 1.03 Tesla. Background pressures of 8.5×10^{-10} torr were maintained in the vacuum system analyzing chamber by a Balzers 330 liter/second turbomolecular pump backed by an Alcatel direct drive roughing pump. Gaseous reagents were set and maintained using a Varian leak valve. Experimental pressures ranging from 2×10^{-7} - 3×10^{-7} torr in the 5 cubic centimeter analyzer cell were measured using a Bayard-Alpert type ionization gauge. The gaseous samples were ionized by electron impact from a 20 millisecond electron beam at an electron energy of 60-70 eV. The filament current ranged from 1.2 - 1.6 μA. Data was collected using the IonSpec OMEGA 50 data system.

The vacuum pyrolysis of used automotive tires was carried out in the preparative flash vacuum pyrolysis apparatus shown in Figure 2 (20). A 30 gram piece of scrap tire made of rubber containing styrene, butadiene, and poly-isoprene was placed in a

quartz pyrolysis tube and pyrolyzed in a Lindberg furnace at temperatures ranging from 300-1000°C in order to determine the optimum temperature for steel recovery. The products were collected in a liquid nitrogen cold trap which was allowed to equilibrate to room temperature following product collection. Upon equilibration the gaseous products were collected in another vial. Separate analysis of the liquid fraction and gaseous products was carried out using FT-ICR. Additional analysis of the liquid product fraction was performed using GC-MS.

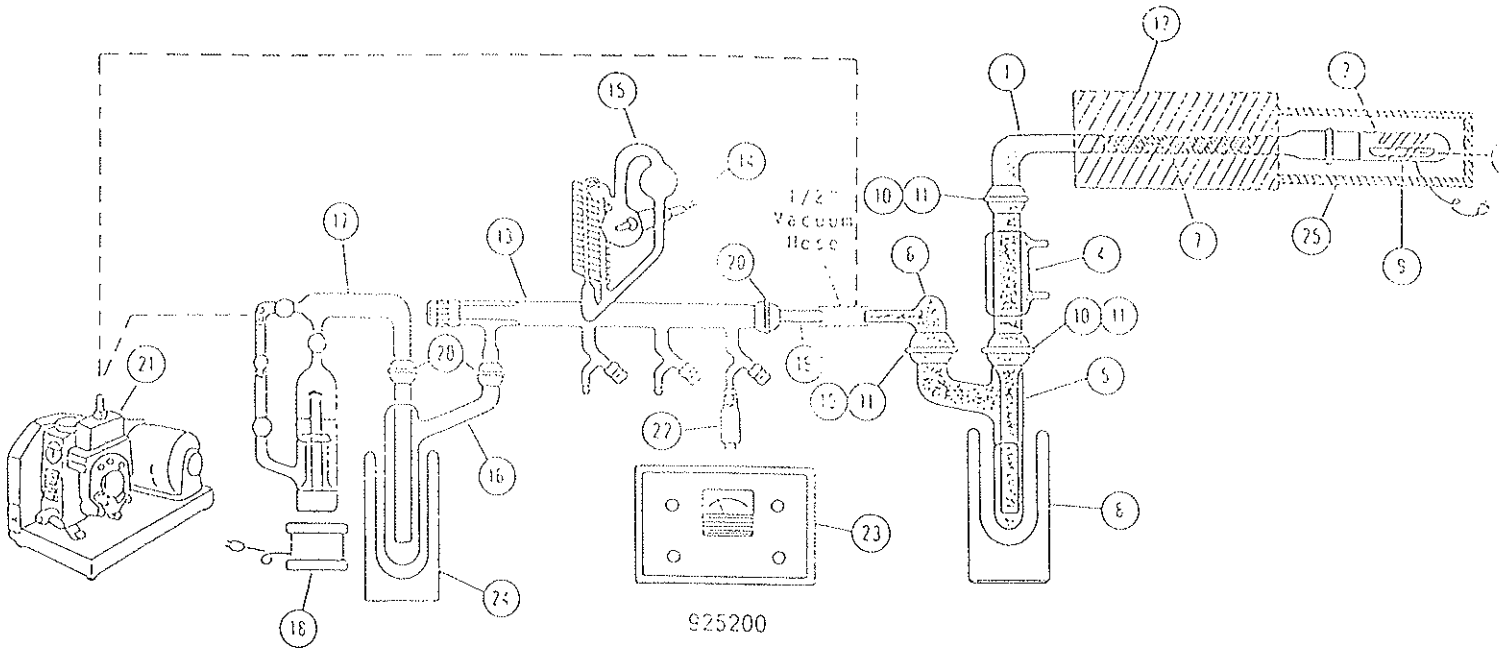

Figure 2. Vacuum Pyrolysis Apparatus

In order to determine the gas phase collision rate for the pyrolysis products, a first order rate approximation was used based on a bimolecular rate law

$$\text{Rate} = k[A][B] \qquad (15)$$

where A and B are the concentration of the reactant ion and the neutral, respectively. A constant pressure of the neutral during a reaction is maintained by the instrument, so the concentration of the neutral, B, can be assumed to be constant resulting in a pseudo-first order reaction.

$$\text{Rate} = k'[A] \qquad (16)$$

Based on a steady state approximation the rate constant for the formation of products can be determined according to equation 17.

$$\text{Ln}(A/A_0) = k't \qquad (17)$$

The resulting k prime was then used to solve for the rate constant k by dividing by the concentration of the neutral gas.

Chemical ionization spectra were obtained using methane gas. The reaction proceeds according to equations 18 and 19 (21).

$$CH_4^+ + CH_4 \rightarrow CH_5^+ + CH_3 \qquad (18)$$

$$CH_5^+ + XH \rightarrow XH_2^+ + CH_4 \qquad (19)$$

Methane is ionized to produce CH_4^+ which then reacts with neutral methane to produce CH_5^+. A reaction occurs between CH_5^+ and the neutral gas molecules, ionizing them by the addition of a proton. In the resulting spectrum, ions of mass M are represented by peaks of M + 1.

RESULTS AND DISCUSSION

Pyrolysis Systems

Prior to the evaluation of a working model for the gas phase reactions that occur in tire pyrolysis, it is essential to identify the products collected in both the liquid and the gas phase following the pyrolysis of tires. The products identified can also be compared to the products formed during combustion processes to evaluate how the pyrolysis process differs from combustion.

Results from the GC-MS analysis of the volatile liquid fraction of pyrolysis products after removal from the equilibrium trap are found in Table 2. The mixture consists of a complicated distribution of many products, largely aliphatic C_8 - C_{10} isomers. Limonene (molecular weight 136), the major product of vacuum pyrolysis (4) comprises 51% of the product distribution. Another important product is cyclohexene, 2,4-hexadiene, or 2,3-dimethyl-1,8-butadiene, (molecular weight 82) which makes up 15% of the liquid fraction. These substituted aliphatic systems contrast significantly to the polycyclic aromatics observed in combustion/fuel pyrolysis processes.

Contained in Figure 3 is a mass spectrum of the initial pyrolysis products obtained through chemical ionization with methane gas. This soft ionization method imparts less energy to the target gas upon ionization, and fewer fragment ions are formed. This allows the molecular ions to be determined more easily. The figure contains the peak (m/z 59) which corresponds to the molecular ion of butene. There is also a small amount of the reactive $C_3H_3^+$ cation (m/z 39), identified as the major precursor ion to soot formation in combustion/fuel pyrolysis processes. The presence of the $C_3H_3^+$ cation

TABLE 2

Products obtained from GC-MS analysis of the liquid fraction of the pyrolysis products

Name	Imperical Formula	%	Molecular weight
Cyclohexene	C_6H_{10}	15	82
2,4-hexadiene			
2,3-dimethyl-1,8-butadiene			
3-Methyl-1-Cyclohexene	C_7H_{12}	2	82
Toluene	C_7H_8	6	92
1,3-Cyclooctadiene	C_8H_{12}	3	108
Ethyl Benzene	C_8H_{10}	3	106
O-Xylene	C_8H_{10}	2	106
Styrene	C_8H_8	8	104
Camphene	$C_{10}H_{16}$	2	136
M-Methylstyrene	C_9H_{10}	2	118
1,2-Dimethyl-3-Ethylbenzene	$C_{10}H_{14}$	4	134
D-Limonene	$C_{10}H_{16}$	51	136

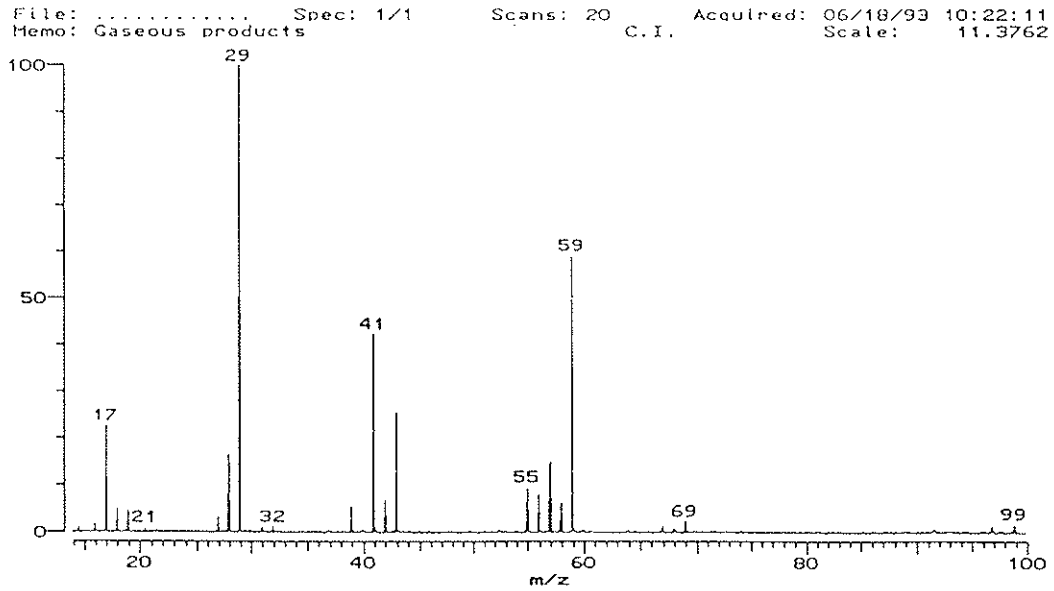

Figure 3. Chemical ionization spectrum of the initial gaseous pyrolysis products

in the chemical ionization spectrum demonstrates that even under low energy conditions this ion is produced quickly and easily from the pyrolysis products. This further supports an ionic mechanism for pyrolysis product formation.

Figure 4 shows an electron impact spectrum of the pyrolysis products obtained at a reaction time of 5 milliseconds. Under the highly energetic conditions, many fragment ions are formed along with the molecular ions. Ions produced include butene, pentene (m/z 67), the $C_3H_3^+$ cation, and additional fragment ions.

In order to evaluate the ability of gas phase reactions to produce large aliphatic systems, the ion-molecule reactions of the ionized gases produced during pyrolysis were investigated. Contained in Figure 5 is a mass spectrum of the products formed following an ion/molecule reaction between the pyrolysis products formed on electron impact (Figure 4) and the neutral pyrolysis products at a reaction time of 10 seconds. The result is a distribution of aliphatic products ranging from $C_6H_9^+$ (m/z 81) to $C_{10}H_{17}^+$ (m/z 137), with the majority of products building upon $C_6H_9^+$ with the successive addition of CH_2. Figure 5 illustrates the capacity of the low molecular weight hydrocarbons generated during pyrolysis to produce larger aliphatic products through ion/molecule reactions.

The distribution shown in Figure 5 can be directly related to many of the major products found in the liquid fraction. For example, the $C_6H_9^+$ cation (m/z 81) corresponds to cyclohexene, hexadiene, or 2,3-dimethyl-1,3-butadiene (molecular weight 82). The $C_{10}H_{17}^+$ cation (m/z 137) corresponds to limonene (molecular weight 136), which makes up over half of the liquid fraction. These results illustrate the effectiveness

of using FT-ICR in simulating the formation of large hydrocarbons from smaller hydrocarbons during the pyrolysis process.

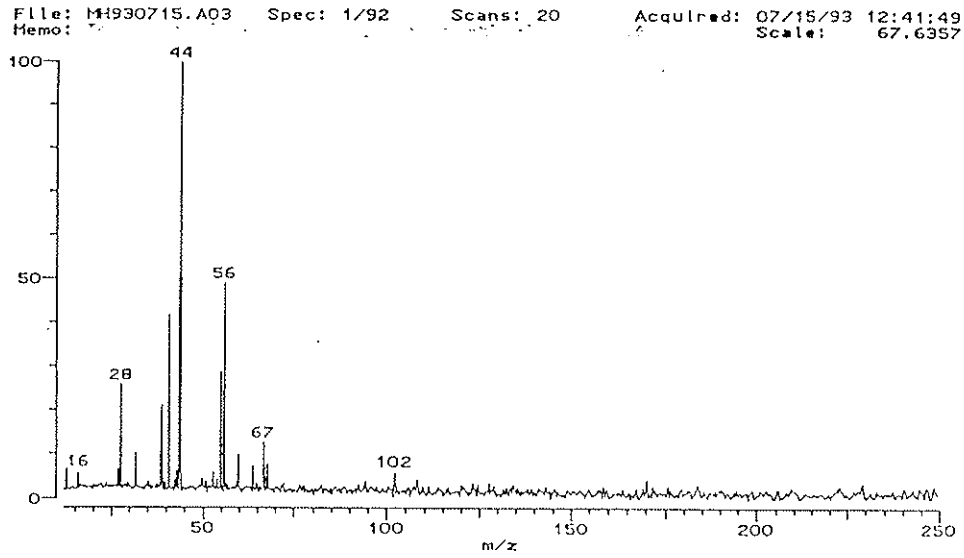

Figure 4. A mass spectrum of the initial gaseous pyrolysis products

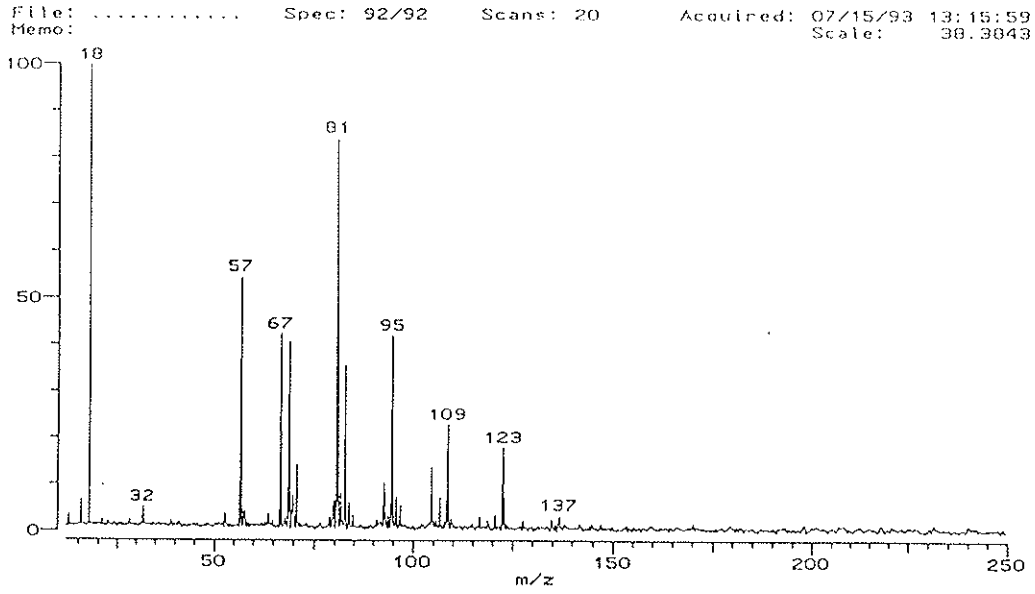

Figure 5. A mass spectrum of the initial gaseous pyrolysis products following an ion/molecule reaction time of 10 seconds

The rates of the ion-molecule reactions were determined by monitoring the intensity of the peaks as a function of time as shown in Figure 6. The reaction rate for the disappearance of the butene (m/z 56) shows that the reaction occurs at approximately the Langeven collision rate. The rapid rate at which the reaction occurs further strengthens the idea of an ionic mechanism driving the formation of products during the pyrolysis process.

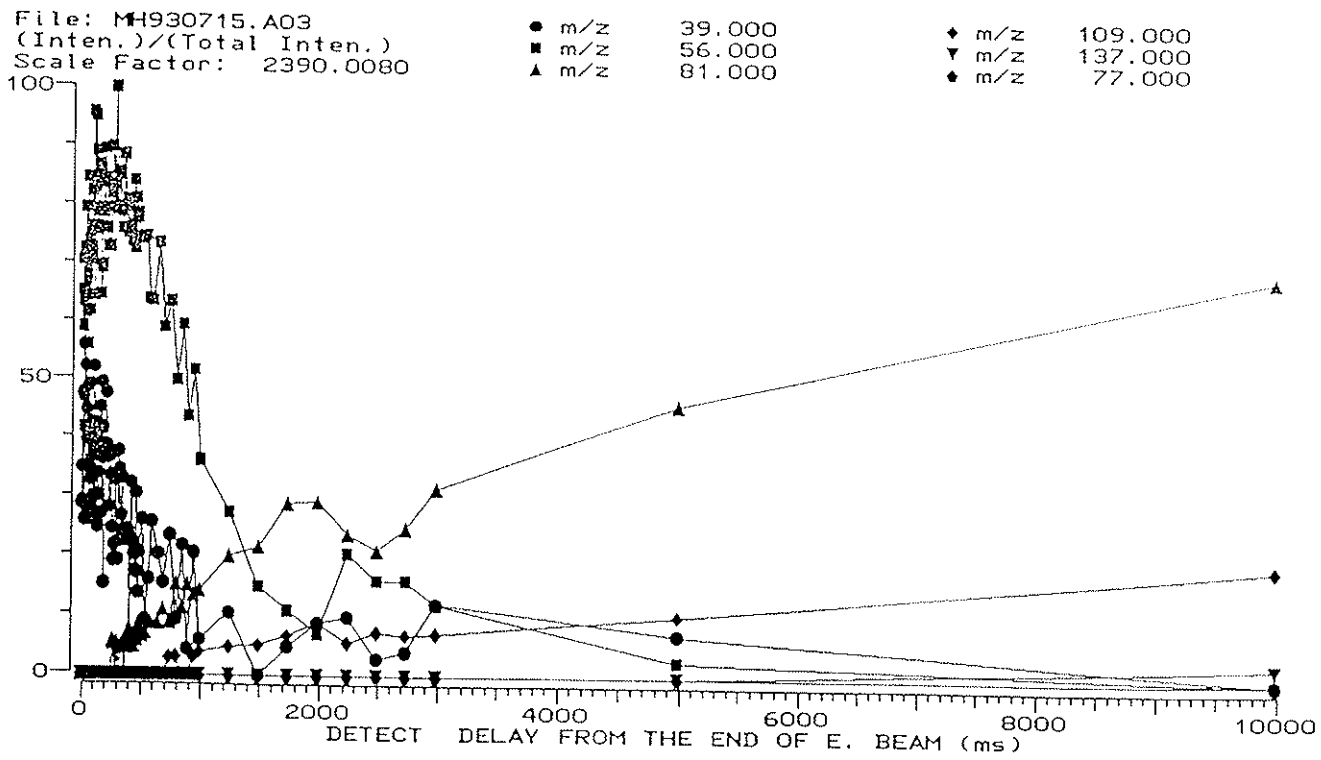

Figure 6. Timeplot for the ion/molecule reaction of the pyrolysis products

Model Systems

Much useful information about the reactions of pyrolysis can be obtained by using a model system with FT-ICR. When using models, reaction parameters can be set and maintained in order to manipulate a specific product distribution. For example, control of reaction time allows reactions which occur very rapidly to be slowed down in order to monitor them more closely. The use of more than one model system within controlled parameters allows similarities and differences between model systems to be observed.

Because of the pervasive nature of conjugated dienes found in natural and artificial rubber, simple conjugated diene compounds were selected to model the pyrolytic gas phase reactions. Specifically, the gas phase reactions of 1,3-butadiene, furan, 1,3-hexadiene, 2,4-hexadiene, and isoprene were evaluated as potential models for scrap tire pyrolysis.

In regard to the products formed during the pyrolysis of scrap tires, the goals of this research are to model the reactions of pyrolysis by modeling aliphatic and aromatic production. By analyzing the reactions of the model systems more information can be gained regarding the mechanism of soot formation during pyrolysis processes and the role that the $C_3H_3^+$ cation plays in this mechanism. Figure 7 illustrates those conjugated diene model systems used and the two reaction pathways which will be discussed.

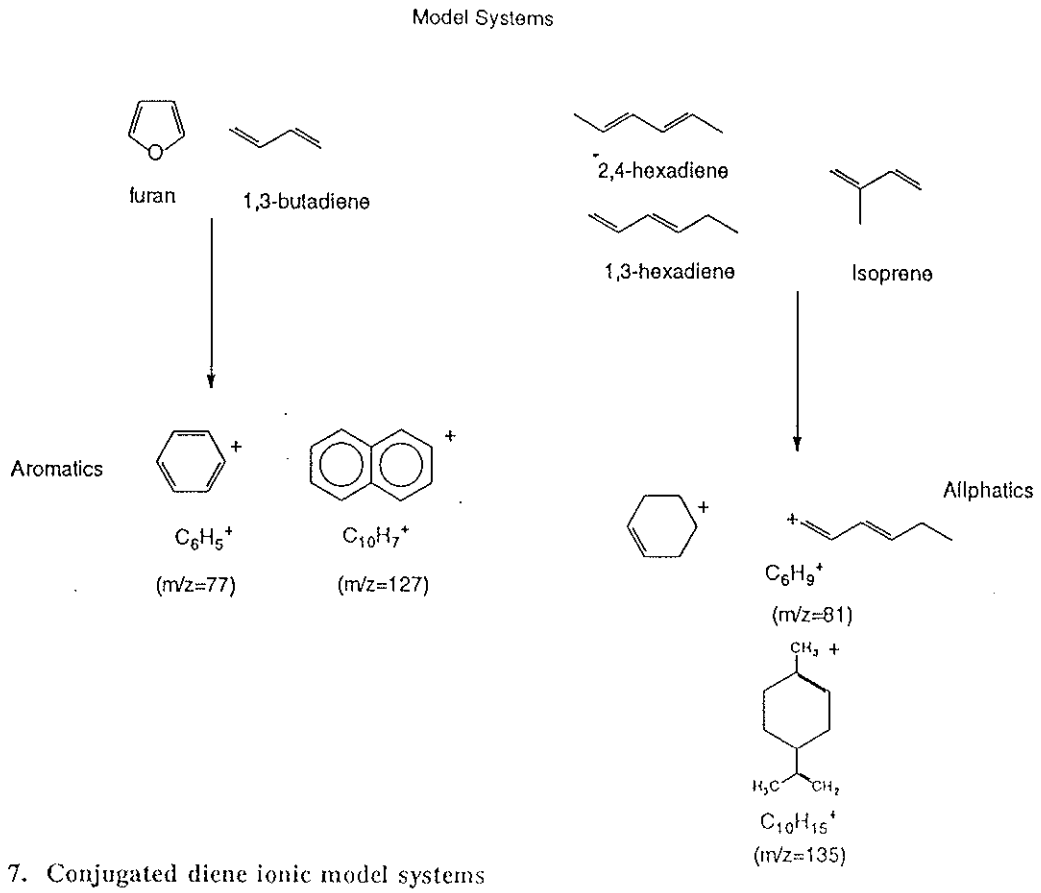

Figure 7. Conjugated diene ionic model systems

AROMATIC PRODUCTION

The production of aromatics is already known to be a significant precursor to the formation of soot particles during the combustion/fuel pyrolysis process. The formation of benzene has been correlated with the formation of soot particles, strengthening the importance of aromatic rings in the growth of soot nuclei (14). The conjugated diene system of furan provides the best illustration of the production of the phenyl cation, $C_6H_5^+$, from the $C_3H_3^+$ fragment ions when studying aromatic production with the conjugated diene model systems.

Contained in Figure 8a is a mass spectrum of furan obtained after a reaction time of 5 milliseconds. The peaks of largest intensity include the molecular ion C_4H_4O (m/z 68) and the $C_3H_3^+$ fragment ion (m/z 39). Upon an ion/molecule reaction time of 700 milliseconds the distribution shown in Figure 8b is produced. Along with the molecular ion, produced through charge exchange of the $C_3H_3^+$ cation with the neutral furan, it is important to observe the production of the phenyl cation $C_6H_5^+$ (m/z 77) through the reactions of the $C_3H_3^+$ cation with neutral furan. The phenyl cation then becomes a precursor ion, producing the larger molecular weight ions represented, $C_9H_7^+$ (m/z 115), $C_9H_9^+$(m/z 117), and biphenyl, $C_{10}H_7^+$ (m/z 127) by reacting with neutral furan.

Figure 9 demonstrates the necessity of the phenyl cation as a precursor to the larger molecular weight products produced during the reaction. The pulse sequence for the continuous ejection of the phenyl cation is shown in Figure 9a. Translational energy was imparted to the phenyl cation increasing its circular orbit beyond the radius of the cell, thereby eliminating it from the reaction. When the reaction was allowed to proceed without the phenyl cation present, the cations of $C_9H_7^+$, $C_9H_9^+$, and $C_{10}H_7^+$ were not produced. This result is observed in Figure 9b.

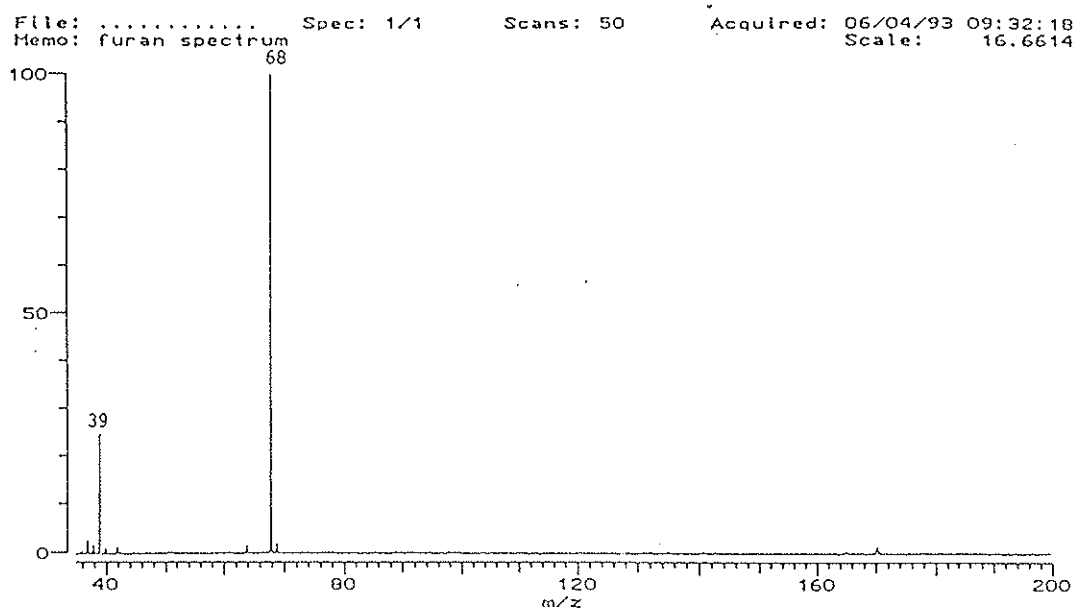

Figure 8a. A mass spectrum of furan at a reaction time of 5 milliseconds

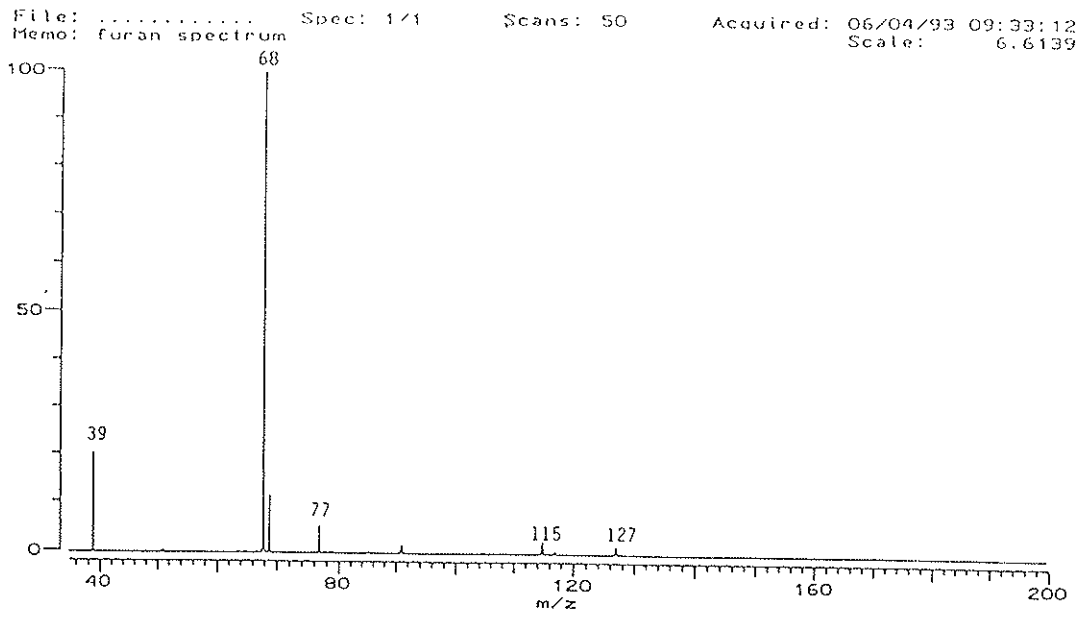

Figure 8b. A mass spectrum of furan at a reaction time of 700 milliseconds

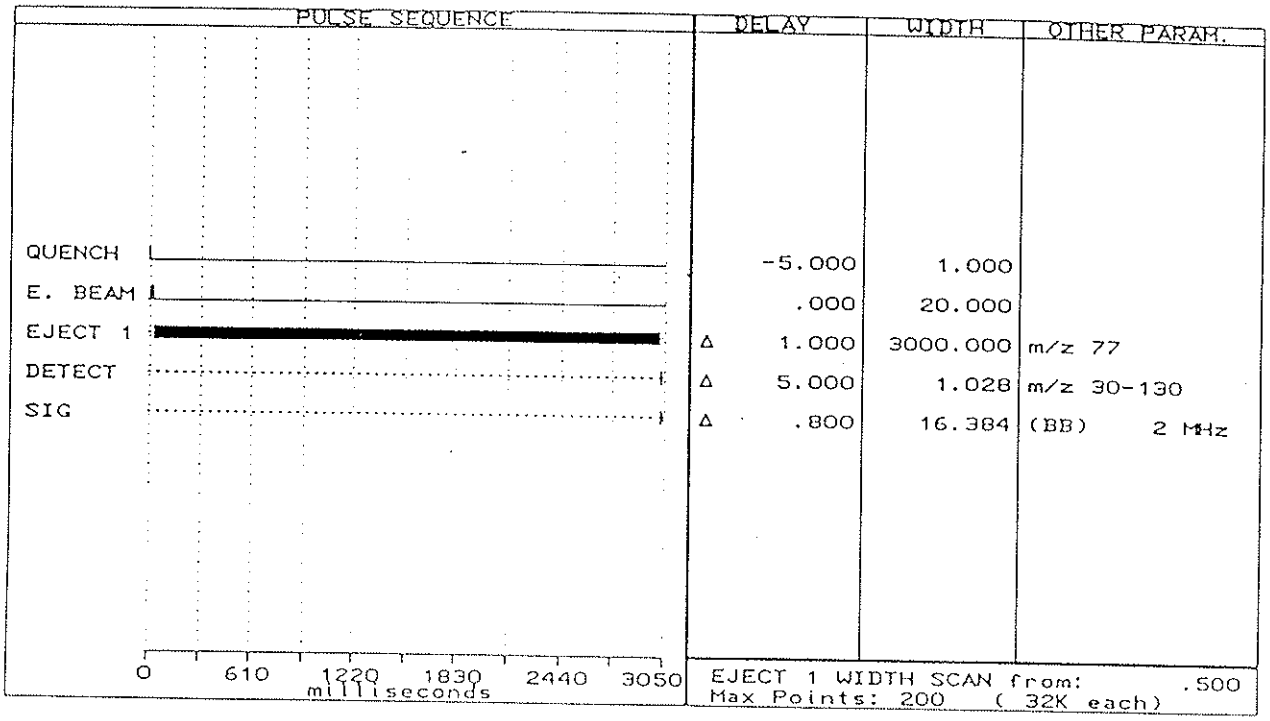

Figure 9a. FT-ICR pulse sequence for the continuous ejection of the phenyl cation from an ion/molecule reaction with neutral furan

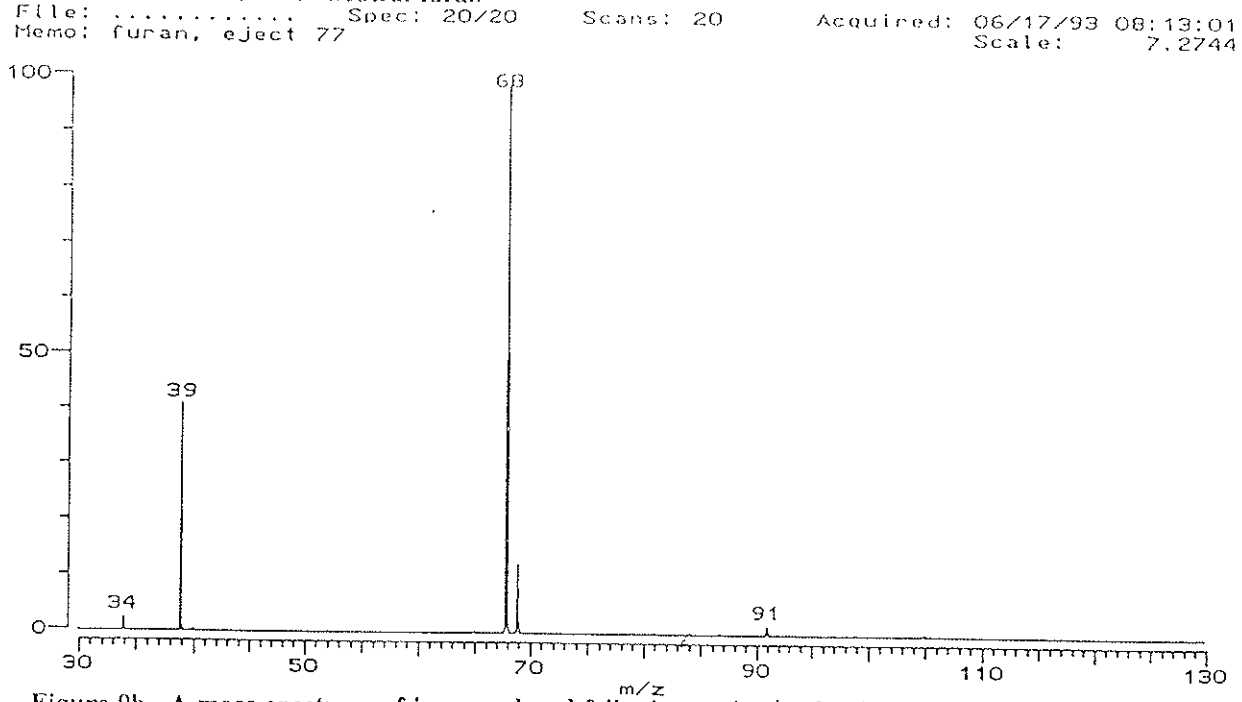

Figure 9b. A mass spectrum of ions produced following an ion/molecule reaction with furan, in which the phenyl cation was not present

The two reaction pathways by which products are formed in the conjugated diene model system of furan are outlined in Figure 10. The phenyl cation is formed through the reactive intermediate $C_7H_7O^+$ (m/z 107), a seven membered ring observed under high pressure conditions (1 x 10^{-3} torr) using a pulse valve. Under low pressure experimental conditions of approximately 2.5 x 10^{-7} torr, this ion falls apart quickly to generate the phenyl cation (22). The phenyl cation then proceeds to react with the neutral furan producing $C_9H_7^+$ (m/z 115), $C_9H_9^+$(m/z 117), and biphenyl, $C_{10}H_7^+$ (m/z 127).

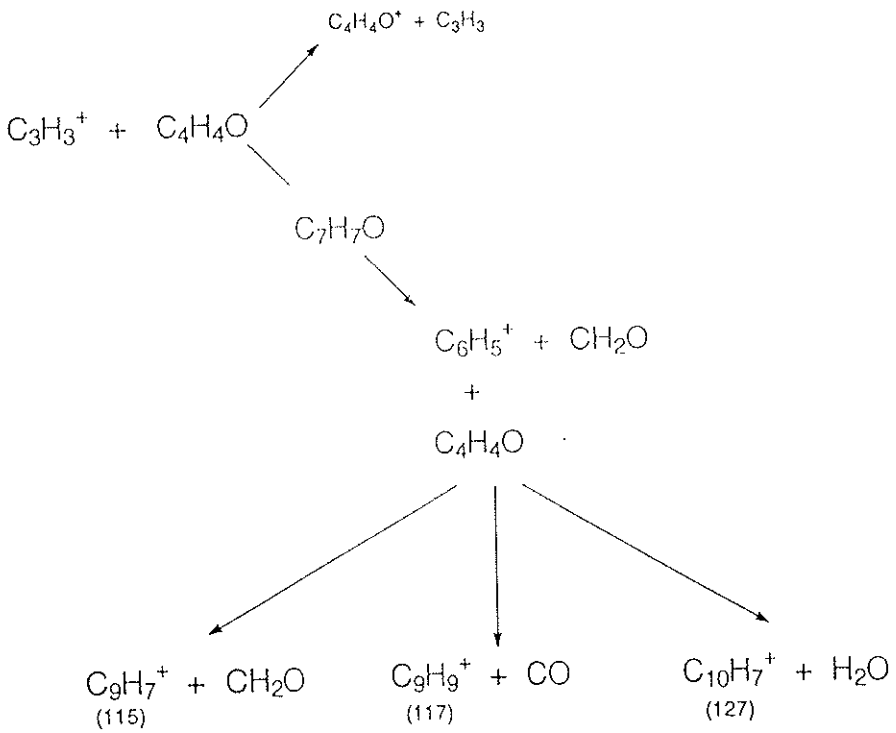

Figure 10. Ion/molecule reaction pathways for the $C_3H_3^+$ cation with neutral furan

ALIPHATIC PRODUCTION

The conjugated diene model system of 1,3-hexadiene illustrates one type of reaction pathway for the production of aliphatic hydrocarbons. The production of aliphatics involves reactions of the $C_3H_3^+$ cation which produce the molecular ion, $C_6H_{10}^+$ (m/z 82), through charge exchange with neutral 1,3-hexadiene. The $C_6H_{10}^+$ cation then produces large substituted aliphatic systems through additional ion/molecule reactions with the neutral gas.

Contained in figure 11a is a spectrum of 1,3-hexadiene following a 5 millisecond ion/molecule reaction. The molecular ion $C_6H_{10}^+$ (m/z 82) is observed along with the $C_3H_3^+$ cation. The distribution of products following a five second ion/molecule reaction time is shown in Figure 11b. The cations represented include: $C_6H_9^+$ (m/z 81), $C_7H_{11}^+$ (m/z 95), $C_8H_{13}^+$ (m/z 109), $C_9H_{15}^+$ (m/z 123), and $C_{10}H_{15}^+$ (m/z 135). Rather than aromatics, these cations are substituted aliphatic systems built upon the $C_6H_9^+$ cation by the subsequent addition of a $-CH_2$ group. This product distribution illustrates that larger aliphatics are formed through the ion/molecule reaction chain.

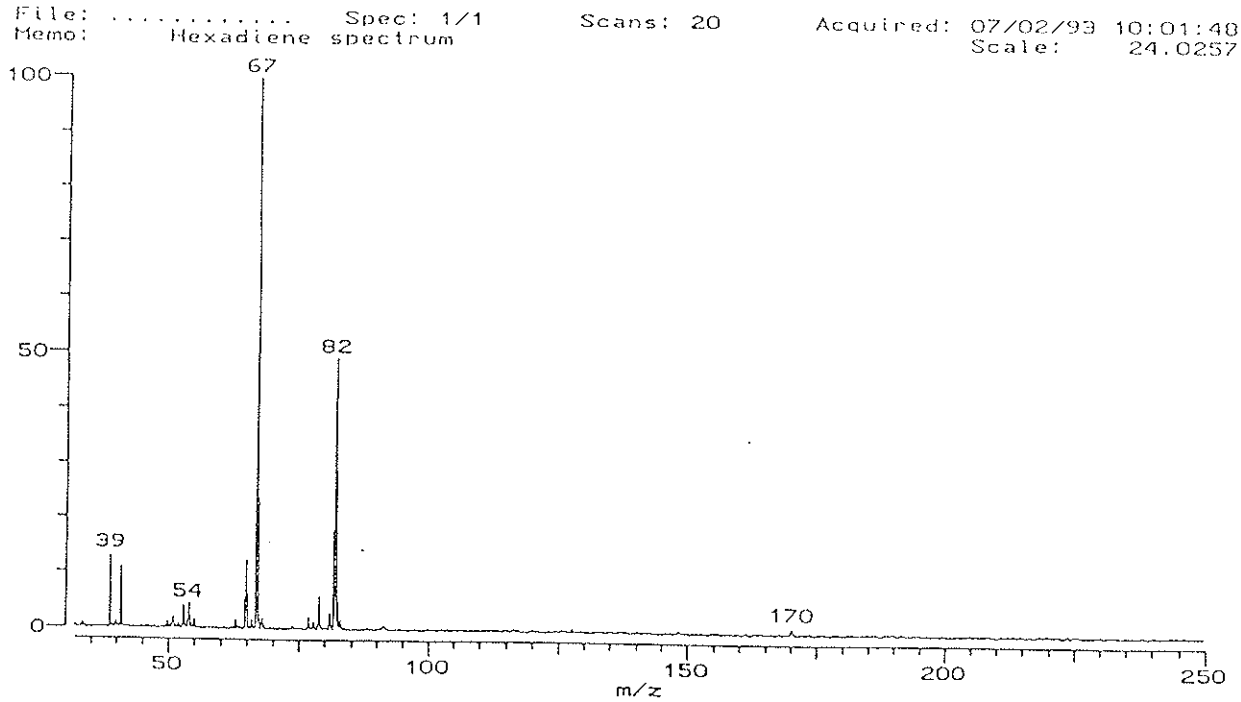

Figure 11a. A mass spectrum of 1,3-hexadiene following a 5 millisecond ion/molecule reaction time

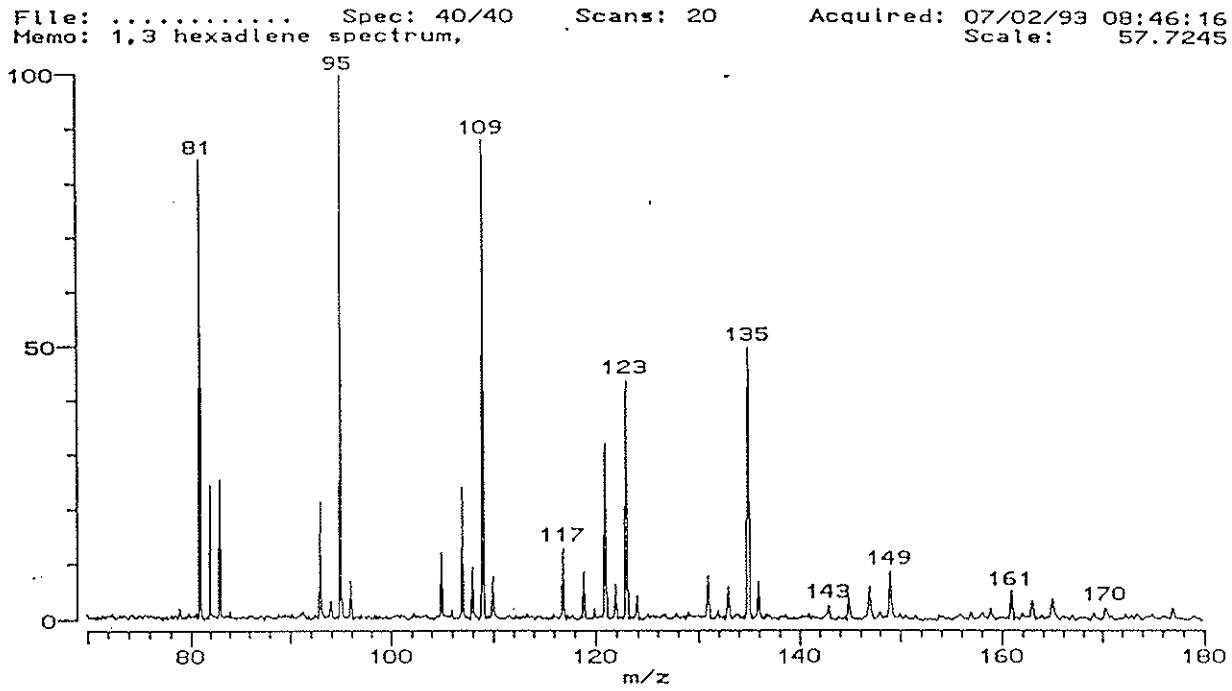

Figure 11b. A mass spectrum of 1,3-hexadiene following an ion/molecule reaction time of 5 seconds

A timeplot of this reaction, shown in Figure 12, demonstrates the ability to measure the relative intensity of the ions as a function of time. Only a small amount of the phenyl cation is produced compared to the reactions of furan. The predominant reaction is that in which the $C_6H_{10}^+$ cation is produced through charge exchange between the neutral 1,3-hexadiene and the $C_3H_3^+$ cation. The molecular ion reaches its peak intensity at a reaction time of less than 250 milliseconds and then begins to be reduced significantly as other ions, particularly $C_6H_9^+$ (m/z 81), are produced. The $C_6H_9^+$ cation becomes the ion of greatest intensity in the product distribution.

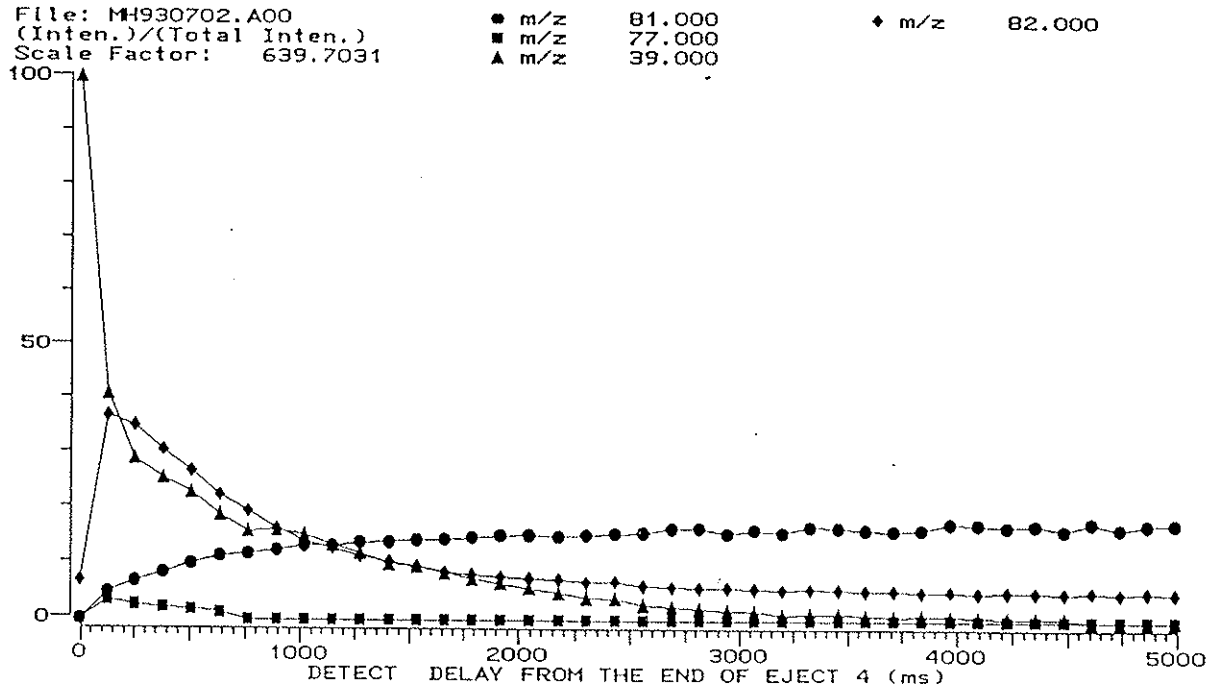

Figure 12. Timeplot for the ion/molecule reaction of 1,3-hexadiene

In order to determine the role of the $C_6H_9^+$ cation in the formation of larger aliphatics, the $C_6H_9^+$ cation was isolated in the FT-ICR cell as pictured in Figure 13a. Following the isolation, an ion/molecule reaction was allowed to take place between $C_6H_9^+$ and neutral 1,3-hexadiene. The resultant distribution, shown in Figure 13b, is consistent with that of Figure 11b. This demonstrates that all of the product ions shown in Figure 11b can be produced from ion/molecule reactions of the $C_6H_9^+$ cation and neutral 1,3-hexadiene.

The necessity of the $C_6H_{10}^+$ cation in the ion/molecule reaction chain that leads to the formation of $C_6H_9^+$ and larger aliphatics is illustrated by Figure 14. Figure 14a shows the pulse sequence for the continuous ejection of the molecular ion as

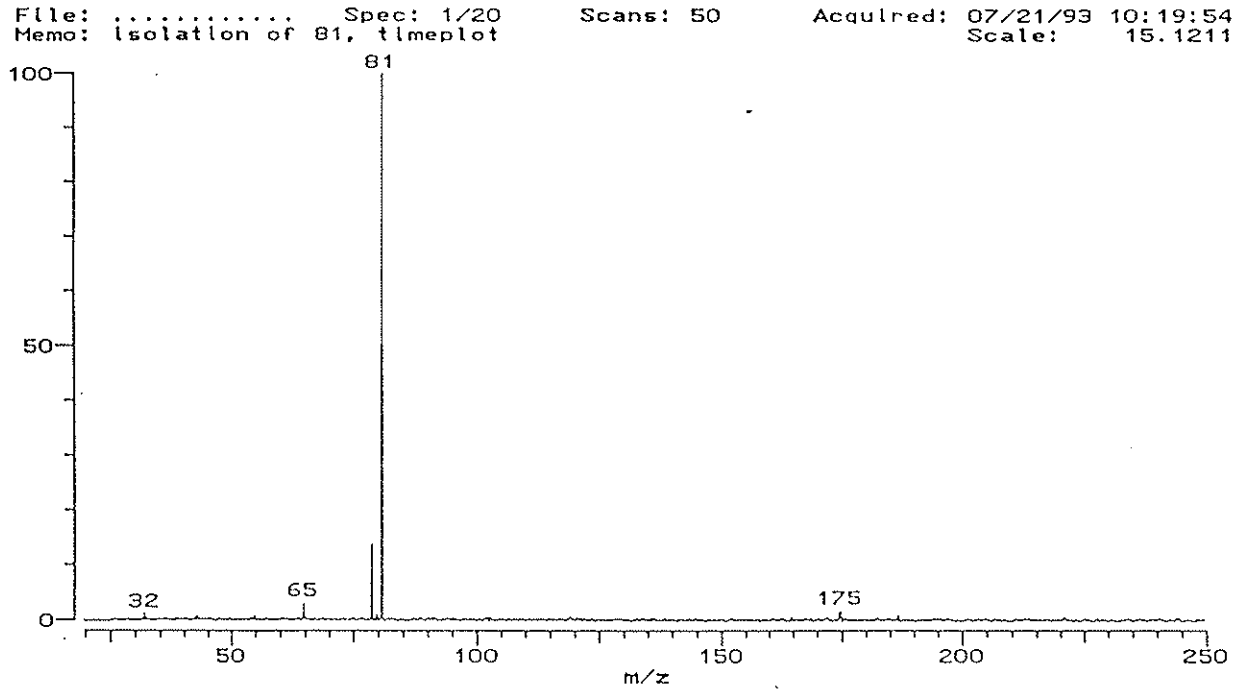

Figure 13a. Isolation of the $C_6H_9^+$ cation (m/z 81) in the FT-ICR cell

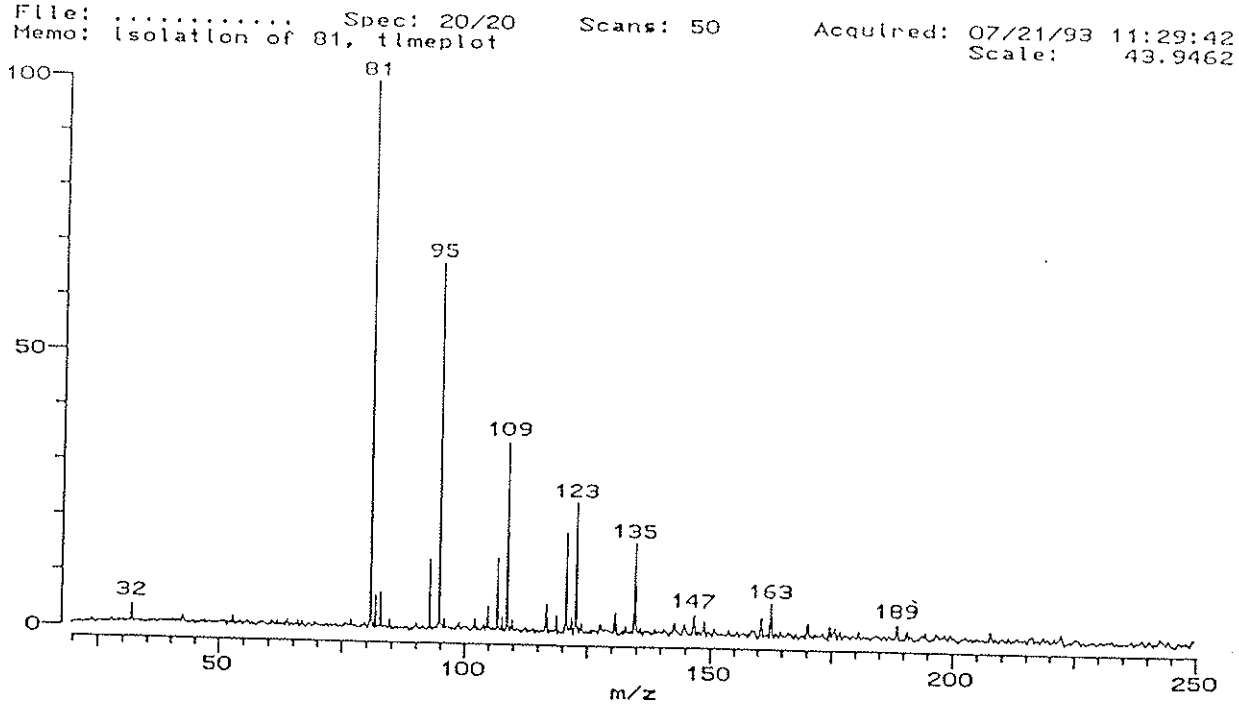

Figure 13b. A mass spectrum following an ion/molecule reaction of the $C_6H_9^+$ cation with neutral 1,3 hexadiene

it was produced through charge exchange during the reaction. A continuous burst of translational energy was applied to the ion, eliminating it from the ICR cell, therefore, it was not present during the ion/molecule reaction time and could not form product ions. The result of this reaction, shown in Figure 14b, is a mass spectrum in which no ions are represented, only noise is observed. The presence of the $C_6H_{10}^+$ cation allows the ion/molecule reaction chain which produces the $C_6H_9^+$ cation and other substituted aliphatics to continue.

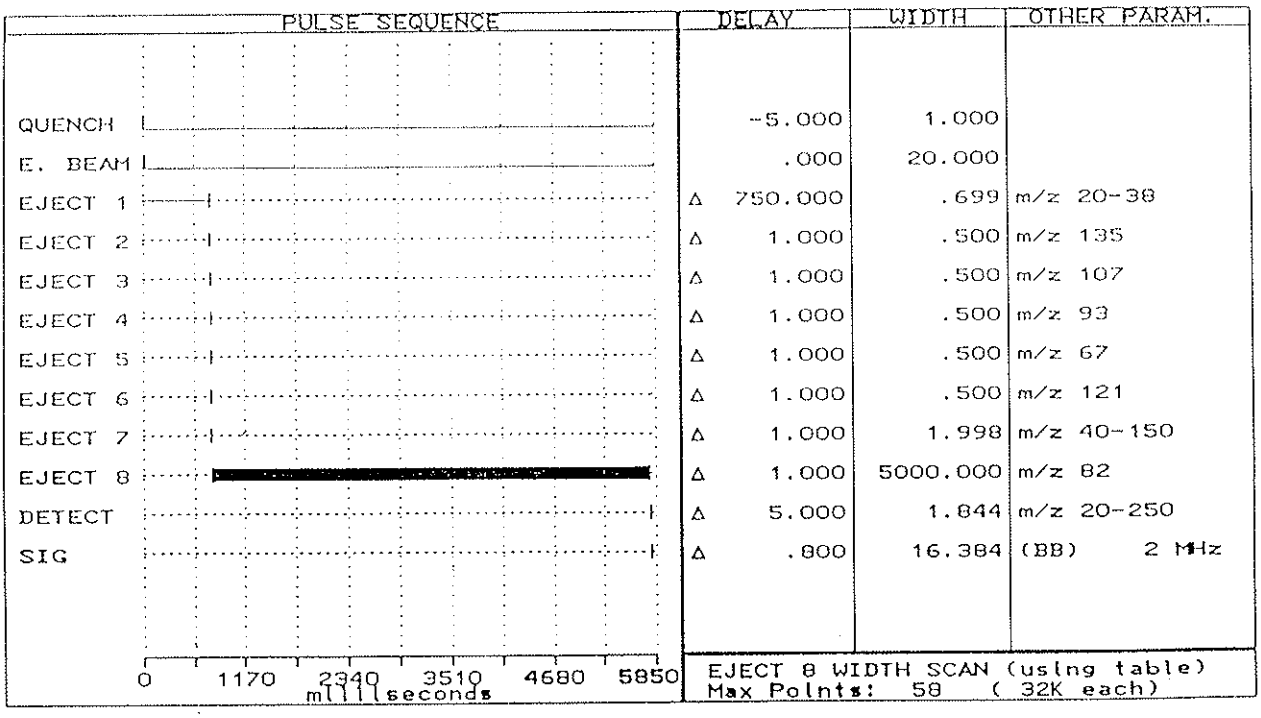

Figure 14a. Pulse sequence for the continuous ejection of the $C_6H_{10}^+$ cation (m/z 82) from the FT-ICR cell, eliminating it from the ion/molecule reaction

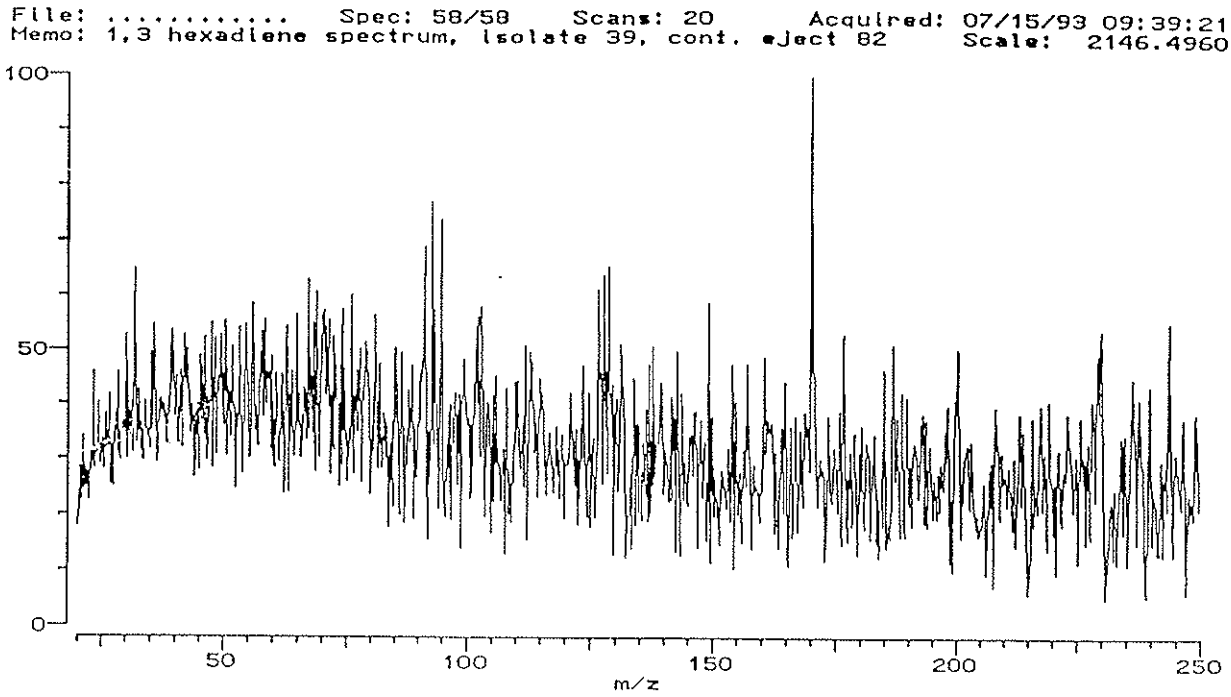

Figure 14b. A mass spectrum of an ion/molecule reaction of 1,3-hexadiene without the presence of the $C_6H_{10}^+$ cation

Outlined in Figure 15 are the pathways for the reactions that lead to the production of aliphatics in 1,3-hexadiene. A small amount of the phenyl cation is produced from the direct reaction of the $C_3H_3^+$ cation with neutral 1,3-hexadiene. However, the most predominant pathway leads to the production of substituted aliphatic systems through the reactions of the $C_6H_{10}^+$ cation which was produced through charge exchange with the $C_3H_3^+$ cation. Reactions of the molecular ion form the $C_6H_9^+$ cation which then reacts with neutral 1,3-hexadiene to produce larger substituted cyclohexenes and hexadienes including $C_7H_{11}^+$ (m/z 95), $C_8H_{13}^+$(m/z 109), $C_9H_{15}^+$ (m/z 123), and $C_{10}H_{15}^+$ (m/z 135).

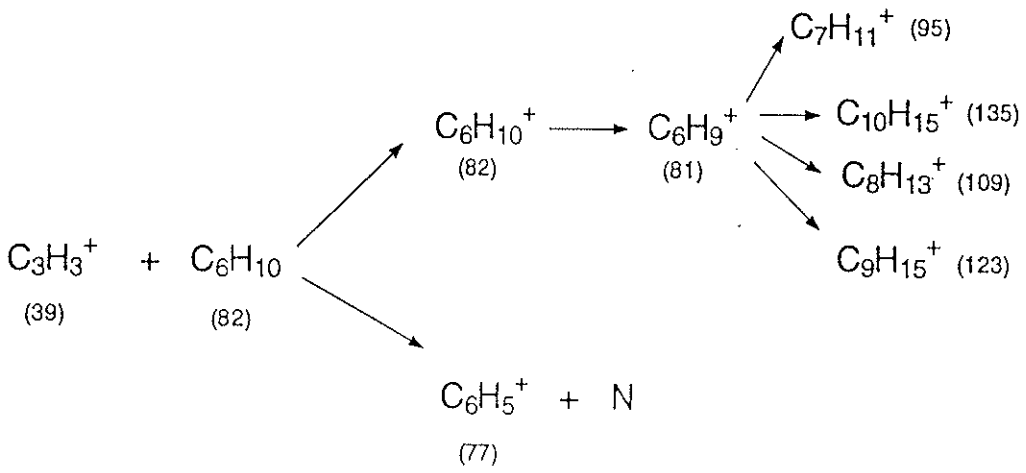

Figure 15. Pathways for the reactions of the $C_3H_3^+$ cation and neutral 1,3-hexadiene

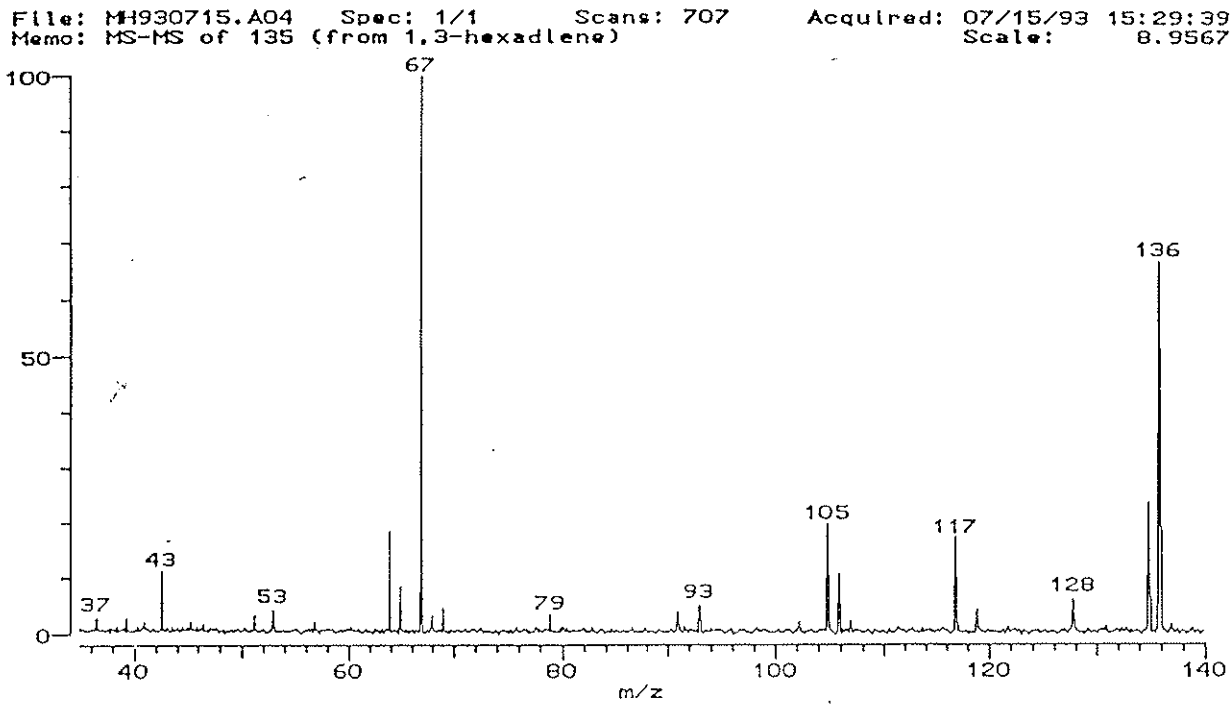

Figure 16b. A mass spectrum of fragment ions following the CID of the $C_{10}H_{15}^{+}$ cation

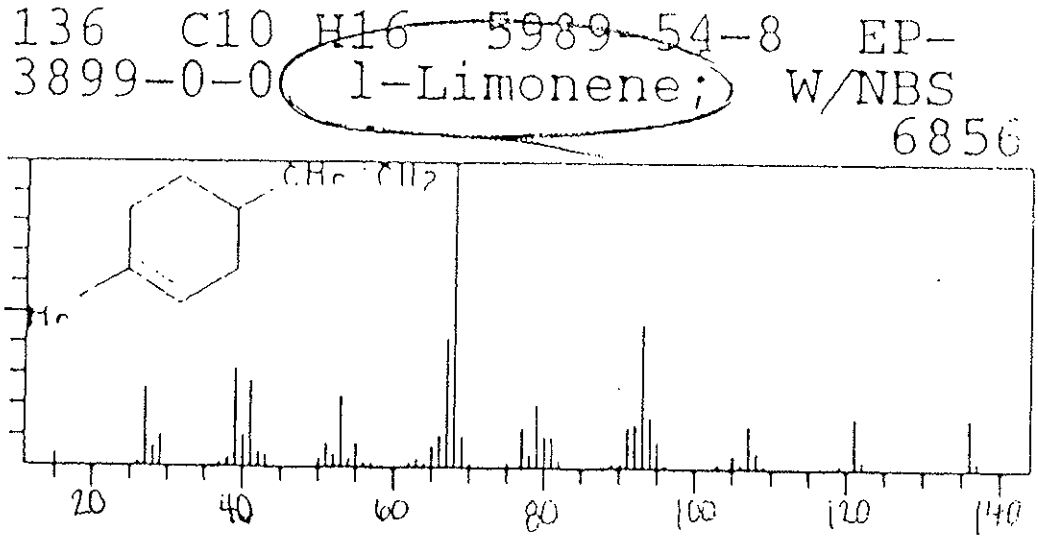

Figure 16c. A mass spectrum of limonene (23)

The $C_{10}H_{15}^+$ cation (m/z 135) present in the ion/molecule reaction spectrum of 1,3-hexadiene corresponds to the molecular weight of limonene (136) the major product of vacuum pyrolysis. A collisionally induced dissociation (CID) experiment was performed in order to determine more about the structure of this particular ion. The pulse sequence for this experiment is illustrated in Figure 16a. The $C_{10}H_{15}^+$ cation was isolated in the FT-ICR cell. Following isolation, a small radio frequency burst with a width of 0.05 milliseconds was applied to the ion. This radio frequency burst imparted translational energy to the ion which caused it to fragment into ions which are represented in the distribution shown in Figure 16b. This distribution correlates with the mass spectrum of limonene shown in Figure 16c.

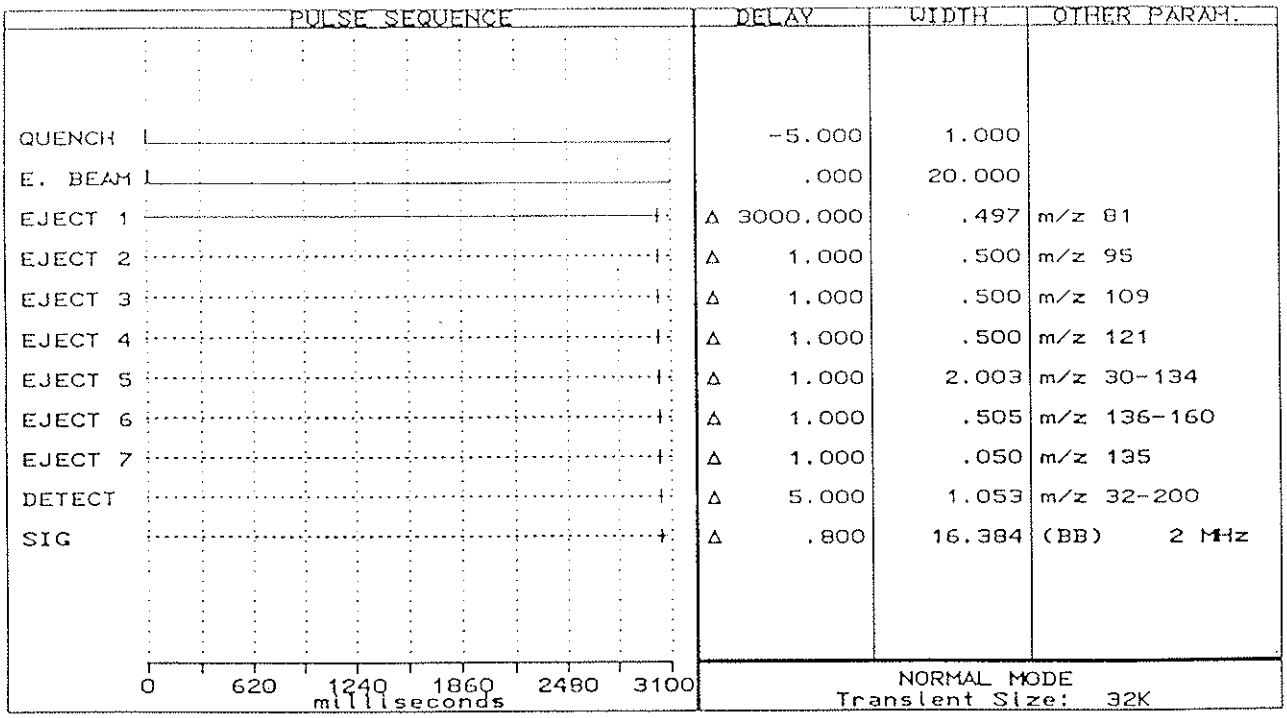

Figure 16a. Pulse sequence for the CID of the $C_{10}H_{15}^+$ cation which was produced through reactions of 1,3-hexadiene

CONCLUSION

These experiments illustrate how FT-ICR can be used to model the gas phase reactions of the pyrolysis process. Small hydrocarbons present in the gaseous pyrolysis products react to form larger hydrocarbons not originally present in rubber. These ions continue to react through ion/molecule reactions to form larger molecular weight products. The specific ions of m/z 81 and m/z 135 correspond to the major products found in the liquid fraction of the pyrolysis products analyzed by GC-MS.

Conjugated diene systems effectively model both aromatic and aliphatic hydrocarbon production. Table 3 shows the relative aromatic ($C_6H_5^+$) vs aliphatic ($C_6H_9^+$) production in each of the five ionic model systems and the pyrolysis gases. The table shows that the small unsubstituted dienes of furan and 1,3-butadiene produce the most aromatic phenyl cation, while the larger substituted systems of 1,3-hexadiene and 2,4-hexadiene produce predominantly aliphatics as do the pyrolysis gases.

The model system of furan illustrates one way in which aromatics are formed. The phenyl cation is formed from reactions of the $C_3H_3^+$ cation and neutral furan through the reactive intermediate $C_4H_4O^+$ (m/z 107). The phenyl cation then acts as a precursor ion, producing the larger cations $C_9H_7^+$, $C_9H_9^+$, and $C_{10}H_7^+$ (biphenyl).

One mechanism for the production of aliphatic systems is illustrated by 1,3-hexadiene. The $C_6H_{10}^+$ cation, produced through charge exchange with the $C_3H_3^+$ cation, acts as the hydrocarbon precursor for the larger substituted aliphatics including the $C_7H_{11}^+$, $C_8H_{13}^+$, $C_9H_{15}^+$, and $C_{10}H_{15}^+$ cations formed through the ion/molecule reaction chain.

Although the $C_3H_3^+$ cation is involved in both aromatic and aliphatic hydrocarbon production, it's role as a precursor ion appears to be different for the two pathways. During aliphatic production the $C_3H_3^+$ cation participates indirectly by forming the $C_6H_{10}^+$ cation through charge exchange. In contrast, the $C_3H_3^+$ cation produces the aromatic phenyl cation through direct reactions with neutral gas molecules.

Consideration of the conjugated diene models in relationship to the actual pyrolysis products indicates that although not present in rubber, 1,3-hexadiene provides the best model for pyrolysis product formation during pyrolysis of tires containing styrene, butadiene, and polyisoprene. Many complicated reactions occur during pyrolysis which result in a distribution of aliphatic product ions. It is very likely that the reaction mechanism for the formation of aliphatics during pyrolysis, although different from that of 1,3-hexadiene is similar. 1,3-hexadiene is a C_6 isomer, and a C_6 isomer is present following ion/molecule reactions of the pyrolysis gases. Figure 18 demonstrates the consistency between the products from pyrolysis (Figure 5) and the products following an ion/molecule reaction of 1,3-hexadiene (Figure 11b). The $C_6H_9^+$ (m/z 81) and $C_{10}H_{15}^+$ (m/z 135) cations found in the spectrum of 1,3-hexadiene also correspond to the major components of the liquid fraction of pyrolysis products.

TABLE 3

Percent production of aromatics vs aliphatics in the

conjugated diene model systems and the pyrolysis gases

Molecule	Percent production of $C_6H_5^+$ m/z 77	Percent production of $C_6H_9^+$ m/z 81
Furan	7.3	1.7
1,3-butadiene	4.4	2.0
isoprene	1.4	29.8
1,3-hexadiene	2.7	13.5
2,4-hexadiene	0.0	11.3
pyrolysis gases	0.0	9.7

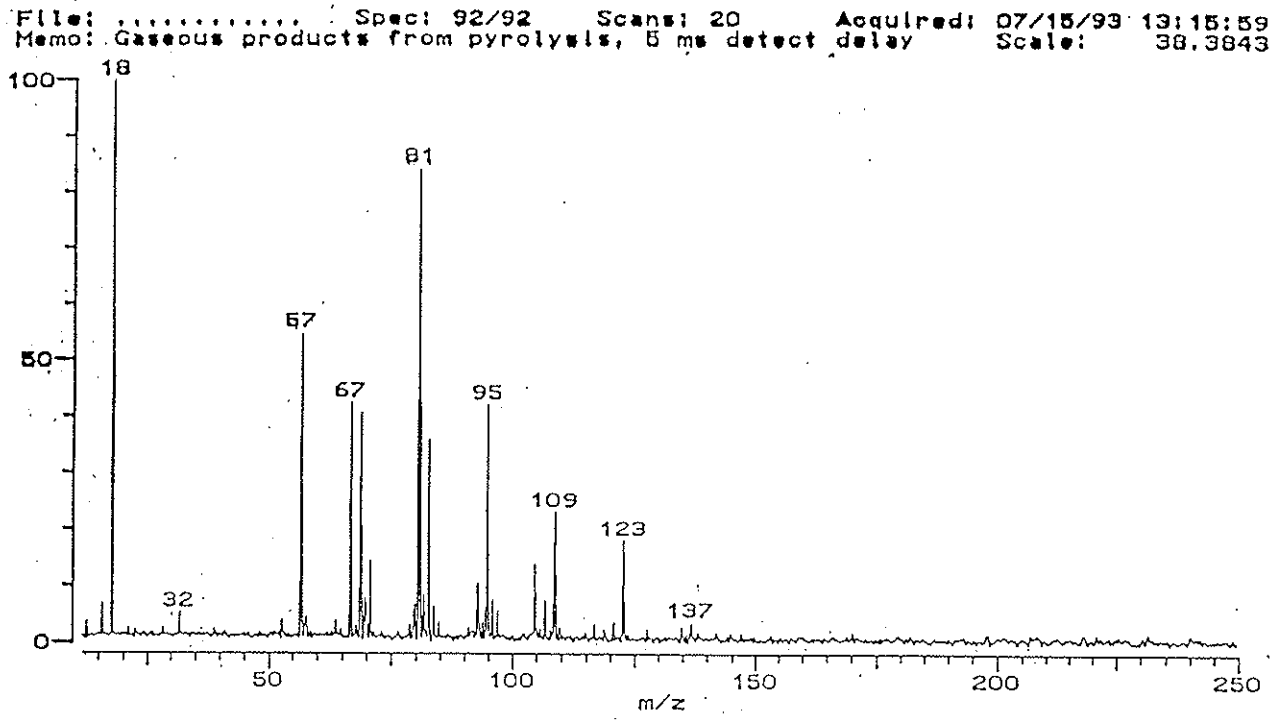

Figure 18a. Product distribution following an ion/molecule reaction of the initial pyrolysis products

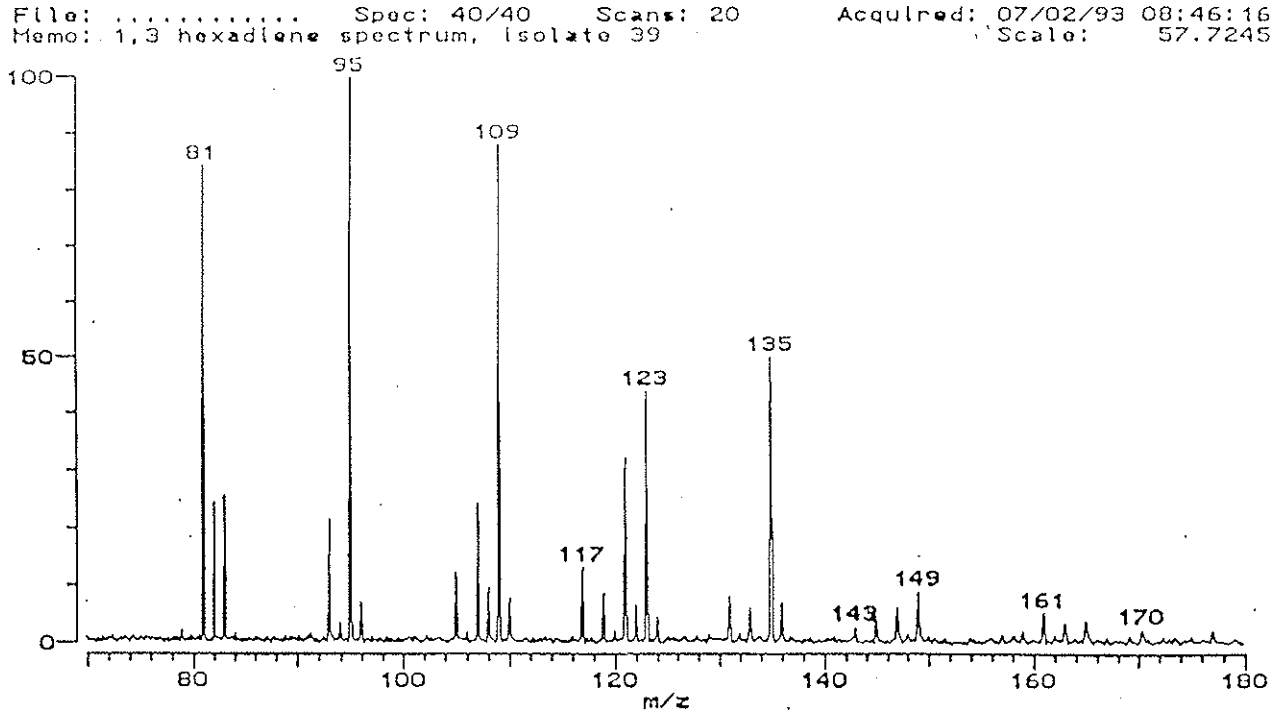

Figure 18b. Product distribution following an ion/molecule reaction of 1,3-hexadiene

ACKNOWLEDGEMENTS

We would like to thank the Small Business Association, the Reuse Recycling Technology Transfer Center, and the University of Northern Iowa Graduate College.

LITERATURE CITED

1. Wingfield, Jr. et. al United States Patent number 4,515,659 May 7, 1985
2. Calcote, H.F. *Combustion and Flame* **1981**, *42*, 215
3. Calcote H.F.; Olson D.B.; Keil, D.G. *Energy & Fuels* **1988**, *2*, 494-504
4. Pakdel, H.; Roy, C.; Aubin,H.; Jean, G.; Coulombe, S. *Environ. Sci. Technol.* **1991**, *25*, 1647
5. Freiser, B.S. *Fourier Transform Mass Spectrometry*
6. Freiser, B.S. *Journal of Chemical Education* **1979**, *56*, 687-691
7. Gross, M.L.; Rempel, D.L. *Science* **1984**, *226*, 261-264
8. Hanson, C.D.; Kerley, E.L.; Castro, M.E.; Russell, D.H. *Analytical Chemistry*, 1989,*61*, 2040-2046
9. Hanson, C.D.; Kerley, E.L.; Russell, D.H. **Recent Developments in Experimental FT-ICR.** *Treatise on Analytical Chemistry.* Second Edition, Part 1, Volume 11, Chapter 2, 1989, Ed. M. Bursey. J. Wiley Publ.
10. Slagle, I.R.; Gutman, D. *Twenty-first Symposium (int.)on Combustion/ The combustion Institute* **1986**, 875
11. Weiner, B.; Williams, C.J.; Heany, D.; Zerner, M.C. *J. Phys. Chem.* **1990**, *94*, 7001
12. Thomas, S.D.; Communal, F.; Westmoreland, P.R. *Preprints of Papers - American Chemical Society* **1991**, *36*, 1449
13. Ausloos, P.J.; Lias, S.G. *J. Am. Chem. Soc.* **1981**, *103*, 6505
14. Kern, R.D.; Woo, C.H. *J. Phys. Chem.* **1987**, *91*, 6291-6296
15. Ozturk, F.; Baykut, G.; Moini, M.; Eyler, J.R. *J. Phys. Chem.* **1987**, *91*, 4361

16. Wiseman, F.L.; Ozturk, F.; Zerner, M.C.; Eyler, J. R. *Int. J. of Chem. Kinet.* **1990**, *22*, 1189-1210

17. Baykut, G.; Brill, F.W.; Eyler, J.R. *Combust. Sci. and Tech.* **1986**, *45*, 233-243

18. Wong, M.W.; Radom, L. *J. Am. Chem. Soc.* **1989**, *111*, 6976

19. Radom, L.; Hariharan, P.C.; Pople, J.A.; Schleyer, P.R. *J. Am. Chem. Soc.* **1976**, *98*, 11

20. Kontes. *Chemistry and Life Sciences Products* **1992**, 375.

21. Bauer, H.H.; Christian, G.D.; O'Reilly, J. E. **Instrumental Analysis.** Allyn and Bacon, Inc. Boston: **1978.** 475.

22. Hammer, M.D.; Rich, M.R.; Burrell, T.; Hanson, C.D. Manuscripts in preparation, University of Northern Iowa, 1993.

23. McLafferty, F.W.; Stauffer, D.B. The Wiley/NBS Registry of Mass Spectral Data. John Wiley and Sons, Inc. New York: **1989** 1:216.